Journal of Sound and Vibration (1999) **221**(1), 1–22
Article No. jsvi.1998.1841, available online at http://www.idealibrary.com.on IDEAL

ON THE STRUCTURAL DAMPING CHARACTERISTICS OF ACTIVE PIEZOELECTRIC ACTUATORS WITH PASSIVE SHUNT

M. S. Tsai and K. W. Wang

Structural Dynamics and Controls Lab, *Mechanical Engineering Department*, *The Pennsylvania State University*, *University Park*, *PA* 16802, *U.S.A.*

(*Received* 12 *September* 1997, *and in final form* 6 *July* 1998)

This paper presents new insights obtained from analyzing the active-passive hybrid piezoelectric network (APPN) concept. It is shown that the shunt circuit not only can provide passive damping, it can also enhance the active action authority if tuned correctly. Therefore, the integrated APPN design is more effective than a system with separated active and passive elements. However, it is also recognized that a systematic design/control method is needed to ensure that the passive and active actions are optimally synthesized. Such a method is developed and presented. The characteristics of the closed-loop system are analyzed.

1. INTRODUCTION

Because of their active and passive damping features, piezoelectric materials have been explored for their active–passive *hybrid* control abilities, which could have the advantages of both the passive (stable, fail-safe, low power requirement) and active (high performance, feedback or feedforward actions) systems. An active–passive hybrid piezoelectric network (APPN) concept has been proposed [1–4] for this purpose. This actuator configurations integrates piezoelectric materials with an active voltage source and a passive R (resistance) L (inductance) shunting circuit (Figure 1). On one hand, structural vibration energy can be transferred to and dissipated in the tuned shunting circuit passively. On the other hand, the control voltage will drive the piezo-layer, through the circuit, and actively suppress vibration of the host structure. Feasibility studies have demonstrated [1–4] that such an APPN-based adaptive structure could suppress vibration and noise radiation effectively, and could achieve better performance with less control effort as compared to a purely active system.

0022–460X/99/110001 + 22 $30.00/0

2. PROBLEM STATEMENT AND OBJECTIVE

While previous investigations on APPN have illustrated promising results, there are still some fundamental and important issues that need to be addressed. These items are summarized as follows.

(1) While the APPN configuration includes both the active and passive elements, the interactions between these elements are not clear. Do the passive elements always complement the active actions?

(2) If the active and passive elements do not always complement each other, should we separate them? In other words, if we separate the active and passive elements, will the active–passive hybrid actions be affected? If they are, will they be enhanced or reduced?

(3) Should we be designing the active and passive control parameters simultaneously or sequentially? Will there be significant differences?

(4) Since the APPN is conceptually an active–passive hybrid tuned damper, it should have bandwidth limitations. How would this issue affect the design?

The objective of this investigation is to address the fundamental issues presented above. In other words, we want to provide more insight and basic understandings to the APPN configuration, and eventually achieve a truly beneficial active–passive hybrid structure for the purpose of vibration suppressions.

3. SYSTEM MODEL

For the purpose of discussion, a cantilever beam partially covered with a pair of PZT (lead zirconate titanate ceramics) actuator–sensor layers is used to illustrate the concept. A schematic of the configuration is shown in Figure 2. The actuator is connected to an external voltage source in series with an RL circuit. The sensor layer is mounted on the other side of the beam at the same axial location.

The system equation is derived based on the following assumptions: (1) the poling direction of the PZTs is in the positive w-direction; (2) the rotational inertia is negligible; (3) only uni-axial loading of the PZTs in the u-direction is considered; (4) the piezoelectric material layers are thin and short compared to the beam; (5) the applied voltage is uniform.

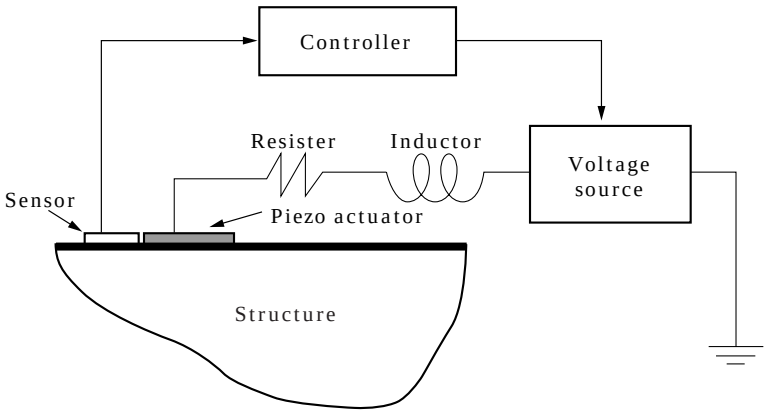

Figure 1. Adaptive structure with active–passive hybrid piezoelectric networks.

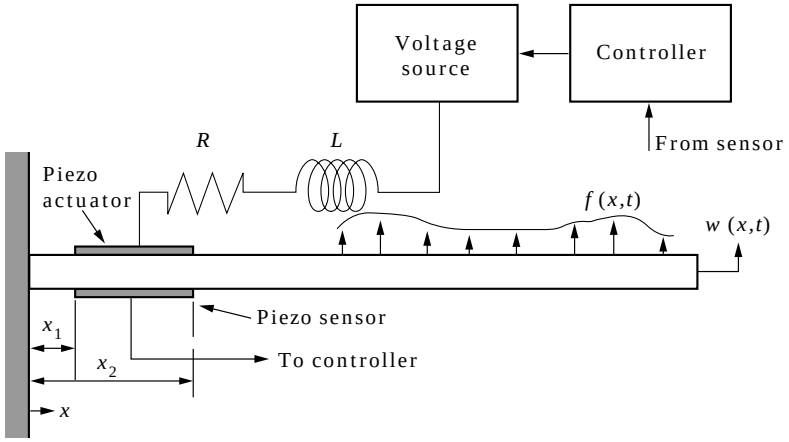

Figure 2. Schematic of a cantilever beam with APPN.

Using Hamilton's Principle, one can construct

$$\int_{t_1}^{t_2} [\delta T_b - \delta U_b - \delta U_c + \delta W_v]\,\mathrm{d}t = 0, \tag{1}$$

where T_b is the beam kinetic energy, U_b is the beam strain energy, U_c is the mechanical and electrical energy of the piezoelectric material, and δW_v is the virtual work term.

For one-dimensional structure with uni-axial loading, the constitutive equation of the piezoelectric material [5] can be written as

$$\begin{bmatrix} \tau \\ E_v \end{bmatrix} = \begin{bmatrix} C_{11}^D & -h_{31} \\ -h_{31} & \beta_{33} \end{bmatrix} \begin{bmatrix} \varepsilon \\ D \end{bmatrix}, \tag{2}$$

where D is the electrical displacement (charge/area in the transverse direction), E_v is the electric field (volts/length along the transverse direction), ε is the mechanical strain in the x-direction, and τ is the material stress in the x-direction. C_{11}^D is the elastic stiffness, β_{33} is the dielectric constant, and h_{31} is the piezoelectric constant of the PZT. Based on the above constitutive equation, and assuming D is constant along the PZT thickness for thin materials, one can derive

$$\begin{aligned} U_c &= \frac{1}{2}\int_V (\tau\varepsilon + E_{va}D_a)\,\mathrm{d}V + \frac{1}{2}\int_V (\tau\varepsilon + E_{vs}D_s)\,\mathrm{d}V \\ &= \frac{1}{2}\int_0^{L_b} \left[2C_{11}^D I_c \left(\frac{\partial^2 w}{\partial x^2}\right)^2 + 2h_{31}J_c\left(\frac{\partial^2 w}{\partial x^2}\right)D_a \right. \\ &\quad \left. + A_c\beta_{33}D_a^2 + 2h_{31}J_c\left(\frac{\partial^2 w}{\partial x^2}\right)D_s + A_c\beta_{33}D_s^2 \right](H(x-x_1) - H(x-x_2))\,\mathrm{d}x. \end{aligned} \tag{3}$$

The other functions are presented as follows

$$T_b = \frac{1}{2}\int_0^{L_b} \rho_b A_b \left(\frac{\partial w}{\partial t}\right)^2 \mathrm{d}x, \qquad U_b = \frac{1}{2}\int_0^{L_b} E_b I_b \left(\frac{\partial^2 w}{\partial x^2}\right)^2 \mathrm{d}x, \tag{4, 5}$$

$$\delta W_v = V_a(t)\int_0^{L_b} b_s \delta D_a (H(x - x_1) - H(x - x_2))\,\mathrm{d}x$$

$$+ V_s(t)\int_0^{L_b} b_s \delta D_s (H(x - x_1) - H(x - x_2))\,\mathrm{d}x$$

$$+ \int_0^{L_b} \left(f(x, t) - c_b \frac{\partial w(x, t)}{\partial t}\right)\delta w(x, t)\,\mathrm{d}x. \tag{6}$$

Note that the voltage is related to the external circuit:

$$V_a = -L\frac{\mathrm{d}^2 Q_a}{\mathrm{d}t^2} - R\frac{\mathrm{d}Q_a}{\mathrm{d}t} - V_c, \tag{7}$$

$$V_a = E_{va}(h_s - h_b), \qquad V_s = E_{vs}(h_s - h_b), \tag{8}$$

$$Q_a = b_s(x_2 - x_1)D_a, \qquad Q_s = b_s(x_2 - x_1)D_s. \tag{9}$$

Here, $w(x, t)$ is the transverse displacement of the beam, E_b is the beam elastic modulus, C_{11}^D is the piezoelectric elastic modulus with an open circuit, L_b is the beam length, ρ_b is the beam density, b_s is the width of the beam and PZT, h_b is the distance from the beam neutral axis to the outside surface of the beam, h_s is the distance from beam neutral axis to the outside surface of the PZT, A_b, A_c are the cross-sectional area of the beam and PZT, respectively. c_b is the uniform damping constant, and I_b and I_c are the beam and PZT layer moments of inertia, respectively. Also, $J_s = b_s(h_s^2 - h_b^2)/2$, $(x_2 - x_1)$ is the length of the PZT, R is the resistance, L is the inductance, V_c is the external voltage for control, V_s is the sensor voltage, D_a, D_s are the electric displacement of the actuator and sensor, respectively. Q_a, Q_s are the electric charge of the actuator and sensor, E_{va}, E_{vs} are the electric field of actuator and sensor, respectively. $f(x, t)$ is the external load distribution, and H is the Heaviside's function. The other parameters are defined in Appendix B.

Substituting the above equations into Equation (1) and further assuming that the field within and electrical displacement on the surface are uniform for the piezoelectric material, one can derive the system model. The structure equation is

$$\rho_b A_b \frac{\partial^2 w}{\partial t^2} + c_b \frac{\partial w}{\partial t} + E_b I_b \frac{\partial^4 w}{\partial x^4} + \left(2C_{11}^D I_c \frac{\partial^4 w}{\partial x^4} + h_{31} J_c \frac{\partial^2 D_a}{\partial x^2}\right)(H(x - x_1)$$

$$- H(x - x_2)) + \left(4C_{11}^D I_c \frac{\partial^3 w}{\partial x^3} + 2h_{31} J_c \frac{\partial D_a}{\partial x}\right)(\delta(x - x_1) - \delta(x - x_2))$$

$$+ \left(2C_{11}^D I_c \frac{\partial^2 w}{\partial x^2} + h_{31} J_c D_a\right)(\delta'(x - x_1) - \delta'(x - x_2)) = f(x, t), \tag{10}$$

where δ is the Dirac delta function and $0 < x < L_b$. The boundary conditions are

$$w(0, t) = \frac{\partial w(0, t)}{\partial x} = \frac{\partial^2 w(L_b, t)}{\partial x^2} = \frac{\partial^3 w(L_b, t)}{\partial x^3} = 0. \tag{11}$$

The actuator circuit equation is

$$\left(V_c + L\frac{\mathrm{d}^2 Q_a}{\mathrm{d}t^2} + R\frac{\mathrm{d}Q_a}{\mathrm{d}t} + \frac{\beta_{33}(h_s - h_b)}{b_s(x_2 - x_1)} Q_a + \frac{h_{31} J_c}{b_s}\frac{\partial^2 w}{\partial x^2}\right)((H(x - x_1) - H(x - x_2)) = 0. \tag{12}$$

Assume an open circuit ($D_s = 0$), the sensor equation is

$$\left(V_s + \frac{h_{31} J_c}{b_s}\frac{\partial^2 w}{\partial x^2} Q_a + \frac{h_{31} J_c}{b_s}\frac{\partial^2 w}{\partial x^2}\right)((H(x - x_1) - H(x - x_2)) = 0. \tag{13}$$

Galerkin's method [6] can be used to discretize equations (10–13) into a set of ordinary differential equations. The comparison functions $\underline{\phi}$ are chosen to be the eigenfunctions of a uniform fixed-free beam.

For the structure, one can obtain

$$M_b \ddot{\underline{\mathbf{q}}} + C_b \dot{\underline{\mathbf{q}}} + K_b \underline{\mathbf{q}} + \frac{h_{31}(h_s^2 - h_b^2)}{2(x_2 - x_1)} [\underline{\phi}'(x_2) - \underline{\phi}'(x_1)] Q_a = \hat{\underline{\mathbf{f}}}. \tag{14}$$

M_b and C_b are the mass and damping matrices derived from the $\rho_b A_b \, \partial^2 w/\partial t^2$ and $c_b \, \partial w/\partial t$ terms in equation (10), respectively. K_b is the stiffness matrix derived from the terms containing $\partial^4 w/\partial x^4$, $\partial^3 w/\partial x^3$ and $\partial^2 w/\partial x^2$ in equation (10); $\hat{\underline{\mathbf{f}}}$ is the external disturbance vector.

For the actuator and sensor circuits,

$$L\ddot{Q}_a + R\dot{Q}_a + \frac{\beta_{33}(h_s - h_b)}{b_s(x_2 - x_1)} Q_a + \frac{h_{31}(h_s^2 - h_b^2)}{2(x_2 - x_1)} [\underline{\phi}'(x_2) - \underline{\phi}'(x_1)]^T \underline{\mathbf{q}} = -V_c, \tag{15}$$

$$\frac{h_{31}(h_s^2 - h_b^2)}{2(x_2 - x_1)} [\underline{\phi}'(x_2) - \underline{\phi}'(x_1)]^T \underline{\mathbf{q}} = -V_s, \tag{16}$$

where $\underline{\mathbf{q}}$, $\underline{\dot{\mathbf{q}}}$, and $\underline{\ddot{\mathbf{q}}}$ are vectors of generalized displacement, velocity, and acceleration. ($\dot{}$) and ($'$) are derivatives with respective to time and x, respectively.

The discretized adaptive structure model, equations (14) and (15), can be expressed in a standard state–space form:

$$\underline{\dot{\mathbf{y}}} = A(R, L)\underline{\mathbf{y}} + B_1\underline{\mathbf{f}} + B_2(R, L)\underline{u}, \tag{17}$$

$$z = C_1\underline{\mathbf{y}}, \qquad \underline{\mathbf{y}} = [\underline{\mathbf{q}}^T \quad Q_a \quad \underline{\dot{\mathbf{q}}}^T \quad \dot{Q}_a]^T, \qquad \underline{u} = V_c,$$

where $\underline{\mathbf{y}}$ is the state vector, $\underline{u}$ is the control input, $\underline{\mathbf{f}}$ is the external disturbance vector. The system matrix, A, and control matrix, B_2, are functions of the passive resistance and inductance.

The system described above has $(N + 1)$ modes, where N is the number of terms in the Galerkin expansion. The $(N + 1)$th mode is due to the passive circuit. Because the comparison functions in the expansion are chosen to be the eigenfunctions of a fixed–free beam, the ith generalized co-ordinate will closely resemble the ith structural modal co-ordinate ($i = 1, 2, 3, \ldots, N$).

The model is used for system analysis and controller development, as discussed in the following sections. The system parameters used for the investigation reported in this paper are shown in Table 1 unless stated otherwise.

4. PRELIMINARY OPEN LOOP SYSTEM ANALYSIS

In this section, the system model is used to investigate the open-loop effects of the circuit parameters (resistance and inductance) have on the passive damping ability and active control authority of the APPN. Also, the APPN is compared to the configuration with separated active and passive elements.

4.1. EFFECTS OF PASSIVE CIRCUIT ELEMENTS ON PASSIVE DAMPING AND ACTIVE AUTHORITY

For a linear system described in the previous section, the overall structural response will be a sum of the response contributed from the excitation force f and the response contributed from the control voltage V_c. We define Y_1 to be the magnitude of the transfer function w_1/f and Y_2 to be the magnitude of the transfer function w_2/V_c. Here, w_1 and w_2 are the responses close to the beam tip ($x = 0{\cdot}92L_b$) caused by the point excitation force at $x = 0{\cdot}95L_b$ and the control

TABLE 1

System parameters

$t_b = 3{\cdot}175$ mm	$b_s = 19{\cdot}05$ mm
$c_b = 0{\cdot}12$ N-s/m^2	$E_b = 7{\cdot}1 \times 10^{10}$ Pa
$C_{11}^D = 7{\cdot}4 \times 10^{10}$ Pa	$h_s = 0{\cdot}0016$ m
$\beta_{33} = 7{\cdot}331 \times 10^7$ volt-m/coulomb	$h_{31} = 7{\cdot}664 \times 10^8$ N/C
$t_c = 0{\cdot}25$ mm	$x_1 = 0{\cdot}0127$ m
$L_b = 0{\cdot}1524$ m	$x_2 = 0{\cdot}0762$ m
$\rho_b = 2700$ kg/m^3	$\rho_c = 7600$ kg/m^3

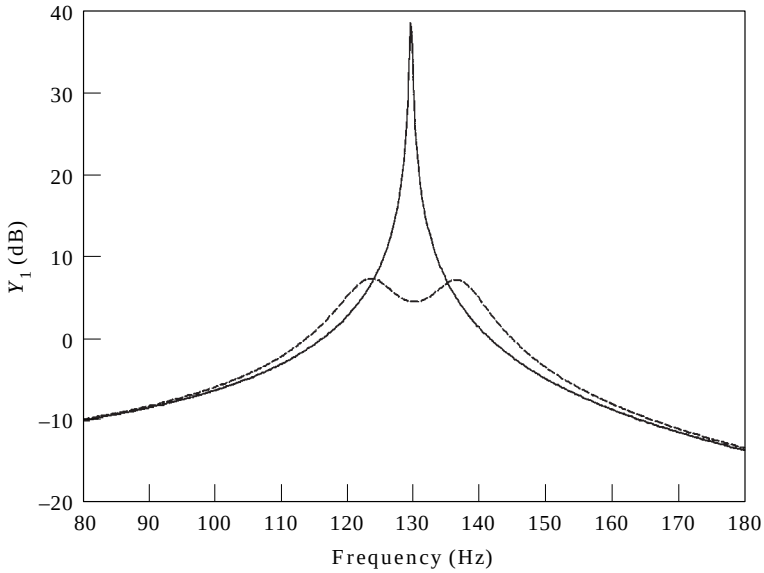

Figure 3. The passive damping index Y_1 : ——, without shunt circuit; – – –, with shunt.

voltage, respectively. With $V_c = 0$, Y_1 represents the structural vibration amplitude without active control. That is, Y_1 is an index of the system's passive damping ability (the smaller the better). On the other hand, Y_2 represents the structural vibration amplitude created by the active actuator. Larger Y_2 indicates that the actuator has more authority to excite the host structure for the given voltage input.

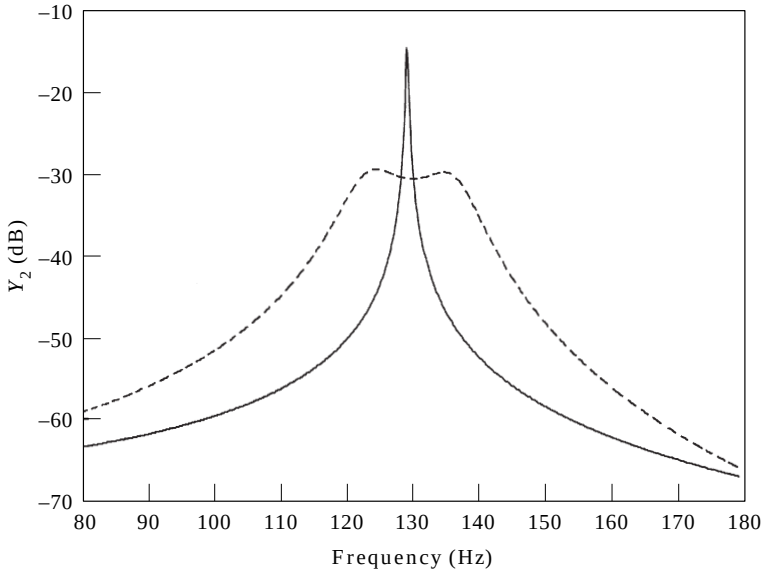

Figure 4. The active control authority index Y_2 for the purely active and APPN systems: ——, purely active; – – –, APPN.

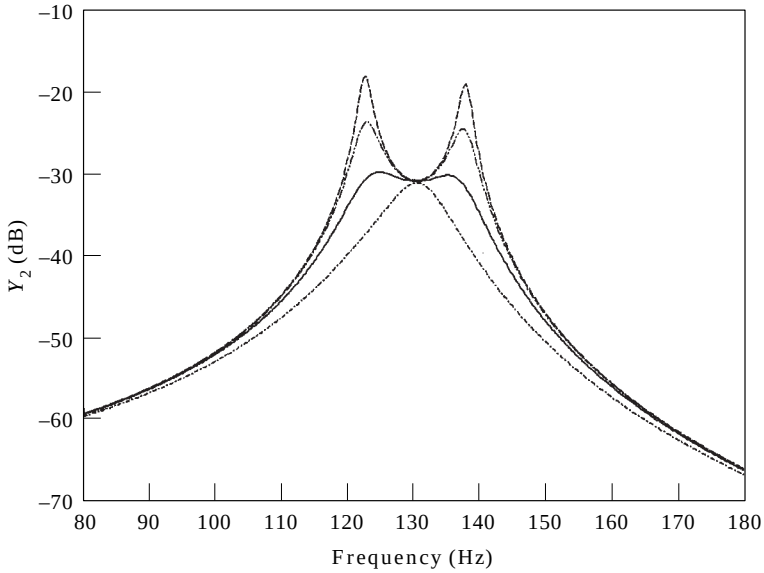

Figure 5. The active control authority index Y_2 with different resistors: – – –, $R = 500\,\Omega$; –··–··–··–, $R = 1{\cdot}0\,\mathrm{K}\Omega$; ——, $R = 2{\cdot}3\,\mathrm{K}\Omega$; -·-·-·-·-·-, $R = 5{\cdot}0\,\mathrm{K}\Omega$.

Thus, Y_2 is used as an index for the system's active control authority (the larger the better).

To illustrate the basic concepts and observations, the first modal response is focused on in the analysis presented in this section, thus only a one-term Galerkin expansion is used. First, the APPN is compared with the purely active system. The R and L values are chosen to be the optimal values for the passive system following the procedure described in Appendix A. Figures 3 and 4 show the passive damping index Y_1 and the active authority index Y_2 for both systems. The Y_1 plot reconfirms that the passive shunt circuit behaves like a tuned resonant damper [7]. In other words, the RL circuit will enhance the passive damping ability around the first resonant frequency. Figure 4 (Y_2 plot) illustrates that the shunt circuit is broadening the actuator active authority bandwidth around the tuned frequency, while reducing the peak value. However, since the R and L values here are chosen to optimize the passive system, it is not obvious that they will be the best for maximizing the active action. For example, while the resistor is designed to dissipate the structure vibration energy, it could be dissipating the control power from the active element as well. This can be observed in Figure 5, where Y_2 is shown to be decreasing with increasing R. In other words, the resistor is reducing the active authority of the actuator.

4.2. INTEGRATED VERSUS SEPARATED ACTIVE AND PASSIVE ELEMENTS

One simple-minded approach to resolve the problem discussed above is to separate the passive shunt circuit from the active source (Figure 6). While this is still an active–passive hybrid configuration, the active and passive elements do not interact directly anymore. This is, we are simply applying active control on an

optimized (tuned circuit) passive system. The structure equation of motion for such a separated configuration is

$$\rho_b A_b \frac{\partial^2 w}{\partial t^2} + c_b \frac{\partial w}{\partial t} + E_b I_b \frac{\partial^4 w}{\partial x^4} + \left(2C_{11}^D I_c \frac{\partial^4 w}{\partial x^4} + h_{31} J_c \frac{\partial^2 D_a}{\partial x^2} + h_{31} J_c \frac{\partial^2 D_s}{\partial x^2}\right)$$

$$\times (H(x - x_1) - H(x - x_2)) + \left(4C_{11}^D I_c \frac{\partial^3 w}{\partial x^3} + 2h_{31} J_c \frac{\partial D_a}{\partial x} + 2h_{31} J_c \frac{\partial D_s}{\partial x}\right)$$

$$\times (\delta(x - x_1) - \delta(x - x_2) + \left(2C_{11}^D I_c \frac{\partial^2 w}{\partial x^2} + h_{31} J_c D_a + h_{31} J_c D_s\right)$$

$$\times (\delta'(x - x_1) - \delta'(x - x_2)) = f(x, t). \tag{18}$$

The shunt circuit and actuator equations are

$$\left(L \frac{\mathrm{d}^2 Q_s}{\mathrm{d}t^2} + R \frac{\mathrm{d}Q_s}{\mathrm{d}t} + \frac{\beta_{33}(h_s - h_b)}{b_s(x_2 - x_1)} Q_s + \frac{h_{31} J_c}{b_s} \frac{\partial^2 w}{\partial x^2}\right)(H(x - x_1) - H(x - x_2)) = 0, \tag{19}$$

$$\left(V_a + \frac{\beta_{33}(h_s - h_b)}{b_s(x_2 - x_1)} Q_a + \frac{h_{31} J_c}{b_s} \frac{\partial^2 w}{\partial x^2}\right)(H(x - x_1) - H(x - x_2)) = 0. \tag{20}$$

The sensor equation is

$$\left(V_s + \frac{\beta_{33}(h_s - h_b)}{b_s(x_2 - x_1)} Q_s + \frac{h_{31} J_c}{b_s} \frac{\partial^2 w}{\partial x^2}\right)(H(x - x_1) - H(x - x_2)) = 0. \tag{21}$$

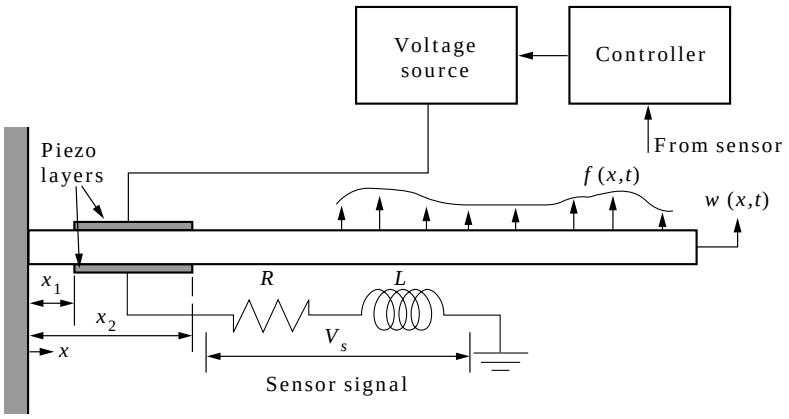

Figure 6. Schematic of a cantilever beam with separated active and passive elements.

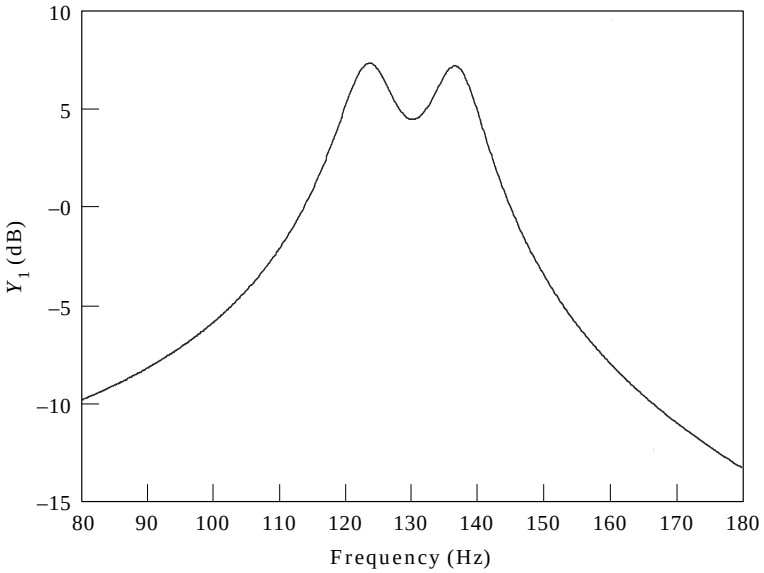

Figure 7. The passive damping index Y_1 for the APPN and separated systems.

Here, the sensor voltage V_s is the voltage across the shunt circuit. Since the two configurations are the same without the active source, the passive damping index Y_1 plot is the same for the two (Figure 7). This implies that the two configurations have the same passive damping ability. However, the active authority index Y_2 plot shows that the APPN can drive the host structure much more effectively than the separated treatment (Figure 8). This is because the circuit can increase the voltage input into the piezoelectric layer around the resonant frequency, even when the

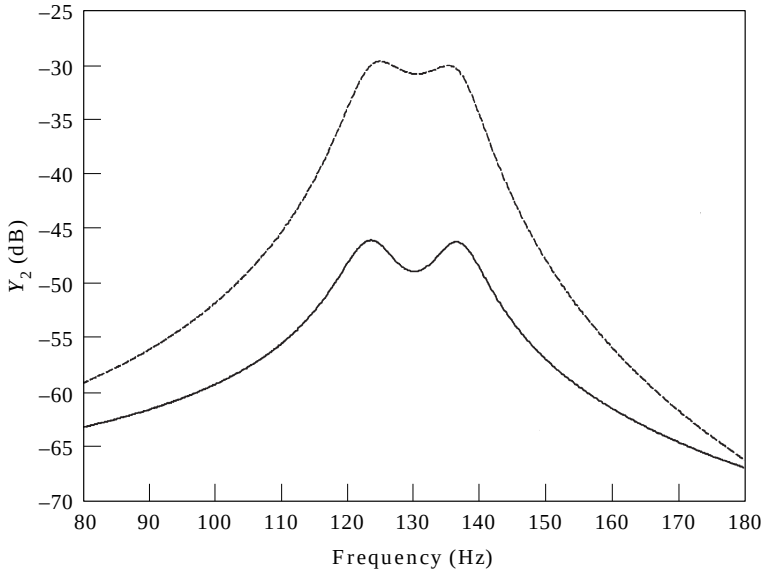

Figure 8. The active control authority index Y_2 for the APPN and separated systems: ——, separated; – – –, APPN.

RL parameters are not optimized for enhancing the active action. This fact illustrates the merit of the integrated configuration over the separated design. Therefore, a sensible thing to do is to use the coupled APPN configuraton with better selected R and L values (instead of the R and L values optimized for the purely passive system). In order to achieve such a purpose, a concurrent design/control method is developed and presented in the next section.

5. ACTIVE–PASSIVE CONTROL LAW DESIGN

A scheme is synthesized to *concurrently* design the passive elements and the active control law. This approach will ensure that the active and passive elements are configured in a systematic and integrated manner. The strategy developed is to combine the optimal control theory with an optimization process and to determine the active control gains *together* with the values of the passive system parameters (the shunt circuit resistance and inductance). The procedure contains three major steps as outlined in the following paragraphs.

5.1. DETERMINE ACTIVE GAINS

In order to examine the system response under different bandwidth excitations, the disturbance is modelled as the result of passing a Gaussian, white noise process through a second order low pass Butterworth filter. The bandwidth of the filter is defined to be the radian cut-off frequency at which the filter output has a 3-dB attenuation of its value at zero frequency. The filter bandwidth is in fact the bandwidth of the external disturbance. The equations that describe such a process are

$$\dot{\underline{\mathbf{s}}} = A_f \underline{\mathbf{s}} + B_f \underline{d}, \qquad \underline{\mathbf{f}} = C_f \underline{\mathbf{s}}, \tag{22}$$

$$\dot{\underline{\mathbf{y}}} = A(R, L)\underline{\mathbf{y}} + B_1 \underline{\mathbf{f}} + B_2(R, L)\underline{u}. \tag{23}$$

The inputs in $\underline{d}$ are Gaussian and white. Here, the mean and spectral density of $\underline{d}$ are given by $E[\underline{d}(t)] = 0$ and $E[\underline{d}(t)\underline{d}^T(\tau)] = D(t)\delta(t - \tau)$. Here, $E[\,]$ is the expectation operator.

By defining an augmented state as $\underline{\mathbf{x}} = [\underline{\mathbf{y}}\ \ \underline{\mathbf{s}}]^T$, the overall system state equations become

$$\dot{\underline{\mathbf{x}}} = \begin{bmatrix} A & B_1 C_f \\ 0 & A_f \end{bmatrix} \underline{\mathbf{x}} + \begin{bmatrix} B_2 \\ 0 \end{bmatrix} \underline{u} + \begin{bmatrix} 0 \\ B_f \end{bmatrix} \underline{d} = A_a \underline{\mathbf{x}} + B_{1a}(R, L)\underline{u} + B_{2a}\underline{d}. \tag{24}$$

With a given set of passive parameters (R and L), the optimal control theory [8] is used to determine the value of the active gains.
The cost function is

$$J_e = \lim_{t \to \infty} E[\underline{\mathbf{x}}^T Q_e \underline{\mathbf{x}} + \underline{u}^T S \underline{u}]. \tag{25}$$

Q_e is a positive-semi-definite weighting matrix chosen to be

$$Q_e = \begin{bmatrix} K_b & & & & & \\ & 0 & & & 0 & \\ & & 0 & & & \\ & & & M_b & & \\ & 0 & & & 0 & \\ & & & & & 0 \end{bmatrix}, \tag{26}$$

Here, $\underline{\mathbf{x}}^T Q_e \underline{\mathbf{x}}$ represents the overall structure energy, while S is the positive-definite weighting matrix on the control inputs. Since the purpose of this paper is to discuss the characteristics of the APPN actuator, the sensor equation is not used here and full state feedback is assumed for demonstration.

With this stochastic regulator control problem, the optimal control gain is given by

$$K_c = S^{-1} {B_{2a}}^T P_r, \tag{27}$$

where P_r satisfies the Riccati equation

$$A_a^T P_r + P_r A_a - P_r B_{2a} S^{-1} B_{2a}^T P_r + Q_e = 0. \tag{28}$$

The closed-loop system thus becomes

$$\frac{\mathrm{d}}{\mathrm{d}t} \underline{\mathbf{x}} = (A_a - B_{2a} K_c)\underline{\mathbf{x}} + B_{1a} \underline{d} = A_{cl} \underline{\mathbf{x}} + \underline{v}, \tag{29}$$

where $\underline{v}$ is Gaussian and white. Here, the mean and spectral density of $\underline{v}$ are given by $E[v(t)] = 0$ and $E[\underline{v}(t)\underline{v}^T(\tau)] = V(t)\delta(t - \tau)$, respectively.

5.2. DETERMINE OBJECTIVE FUNCTIONS

The objective function is selected to be the minimized cost function of the stochastic regulator problem [8]

$$J = \mathrm{Min}\, J_e = \mathrm{trace}(P_l V). \tag{30}$$

P_l is the solution to the following Lyapunov equation:

$$A_{cl} P_l + P_l A_{cl}^T + V = 0. \tag{31}$$

5.3. ITERATION ON ACTIVE GAINS AND PASSIVE PARAMETERS TO MINIMIZE J

Note that for each set of the passive control parameters R and L, there exists an optimal control with the corresponding minimized cost function and control gains. That is, J is a function of R and L. Utilizing a sequential quadratic programming algorithm [9], one can determine the resistance and inductance which further minimze J. As the passive parameters vary, the active gain will be updated as well. In other words, by varying the values of the active gains and passive parameters simultaneously, the "optimized" optimal control can be obtained.

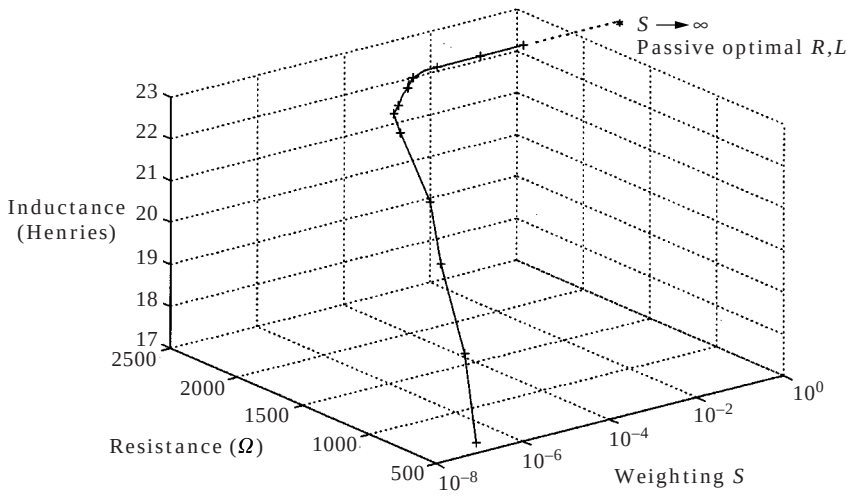

Figure 9. The optimal resistance and inductance for different weighting S.

6. ANALYSIS OF THE OPTIMIZED CLOSED-LOOP SYSTEM

6.1. THE EFFECT OF WEIGHTING

As stated earlier, the optimal resistance and inductance for the active–passive hybrid system may not be the same as the optimal R and L for a purely passive arrangement. In order to evaluate the differences, the optimal R and L for different weightings on control effort are shown in Figure 9. Here, a three term Galerkin's expansion is used and the excitation bandwidth (bandwidth of the Butterworth filter described in section 5.1) is set to be 192 Hz for us to focus on the first mode.

The optimal R and L for the passive case shown in Figure 9 are calculated using the passive optimization process stated in Appendix A. Note that when the weighting on control effort S increases (more limitation on control effort), the optimal R and L values using the concurrent design approach those derived from the passive optimization procedure. This is because the input control effort would be very small under the condition of large S and passive damping is dominating. However, it is seen that the optimal R, L values for the hybrid system depart quite significantly from the R, L values for the purely passive system as the demand on performance increases (i.e., S decreases). This indicates that the simultaneous controller/circuit optimization process is necessary, especially when high system performance is required. It is also shown in Figure 9 that the higher the S, the smaller the resistance and inductance. In order to understand this trend and further illustrate the effect of S on the system characteristics, another set of indexes for passive damping (I_p) and active authority (I_a) are defined as follows:

$$I_p = (J_{p\_pa} - J_{p\_ap})/J_{p\_pa}, \qquad I_a = (J_{a\_ap} - J_{a\_pa})/J_{a\_pa}, \tag{32, 33}$$

where J_{p_pa} and J_{p_ap} represent the total structure energy (potential and kinetic energy) of the purely active and APPN systems under the same level of external disturbances (without active control), respectively. Higher I_p indicates more passive damping ability. J_{a_pa} and J_{a_ap} represent the total structure energy of the

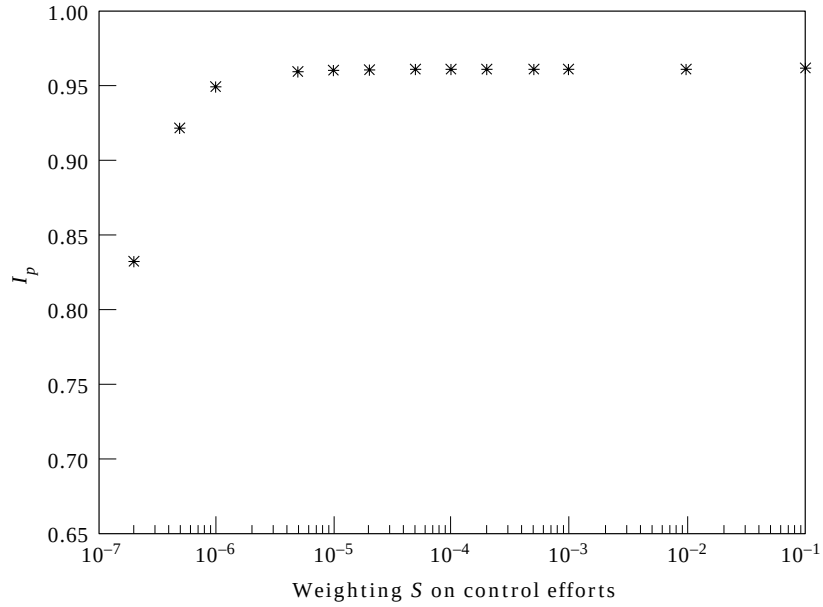

Figure 10. The passive damping I_p for different weighting S.

purely active and APPN systems when the structure is driven by the same level of control voltage (without external disturbance). Larger I_a indicates more control authority. J_{p_pa}, J_{p_ap}, J_{a_pa} and J_{a_ap} can be calculated from equation (A6) in Appendix A. Both the external force and control voltage are modelled as white noise passing through a low pass Butterworth filter with bandwidth of 192 Hz. Figures 10 and 11 show that I_p decreases while I_a increases, as the weighting

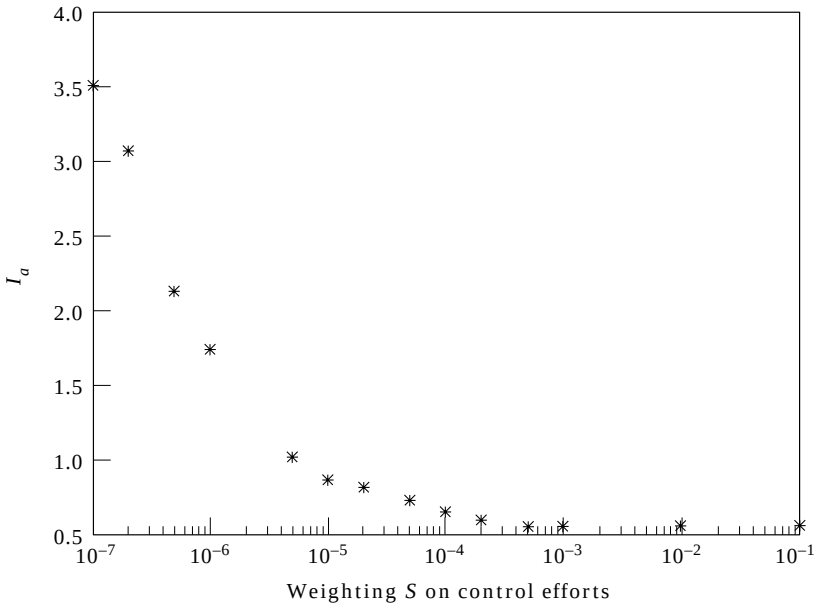

Figure 11. The active authority I_a for different weighting S.

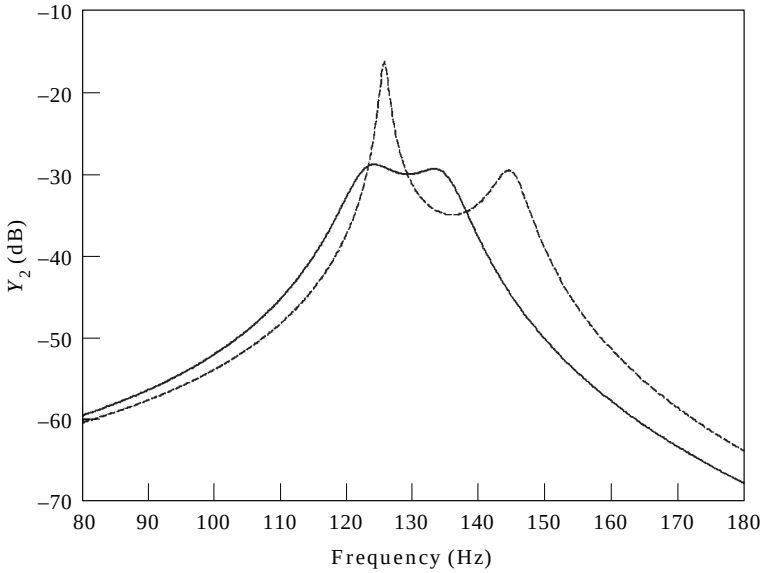

Figure 12. The active control authority index Y_2 for different weighting S: ——, $S=1 \times 10^{-1}$; – – –, $S = 2 \times 10^{-7}$.

S decreases. This implies that when the demand on performance becomes higher (lower S), the optimal R and L values will vary in a direction to increase active authority while reducing passive damping. We therefore examine the frequency response of Y_2 (active authority index) in the cases of high and low weightings S. It is clear from Figure 12 that when the demand on performance is high, R becomes smaller to enhance the active authority peak magnitude, and

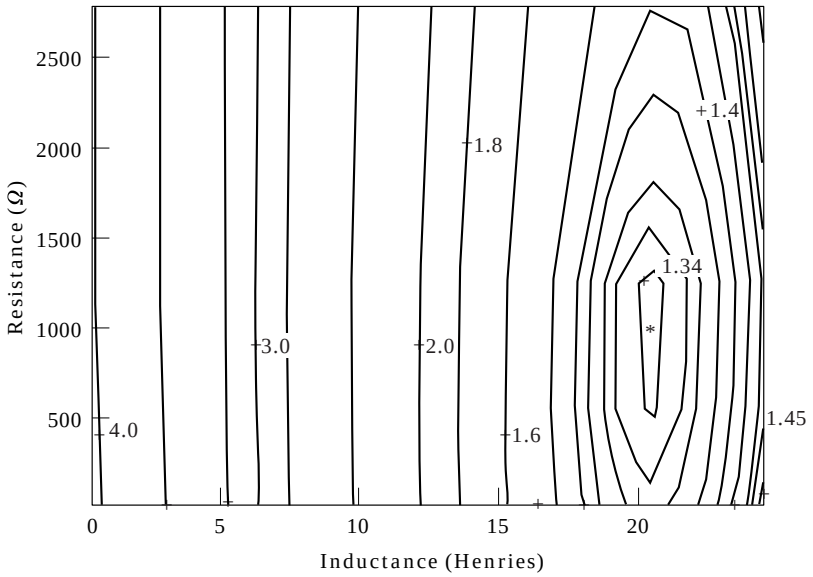

Figure 13. Contour of the cost function J under the excitation bandwidth 190 Hz: *, optimal resistance and inductance; $J = 1{\cdot}335$.

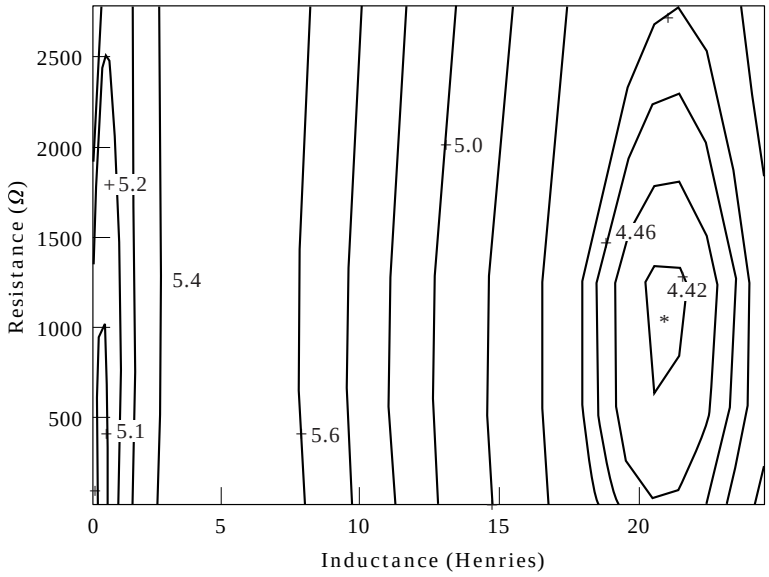

Figure 14. Contour of the cost function J under the excitation bandwidth 560 Hz: *, optimal resistance and inductance; $J = 4{\cdot}414$.

L reduces to push the actuator frequency response up to cover a wider frequency bandwidth.

6.2. THE EFFECT OF EXCITATION BANDWIDTH

In order to examine the APPN system under broadband excitations, a three-mode expansion is used which covers modal frequencies up to 1·97 kHz. The

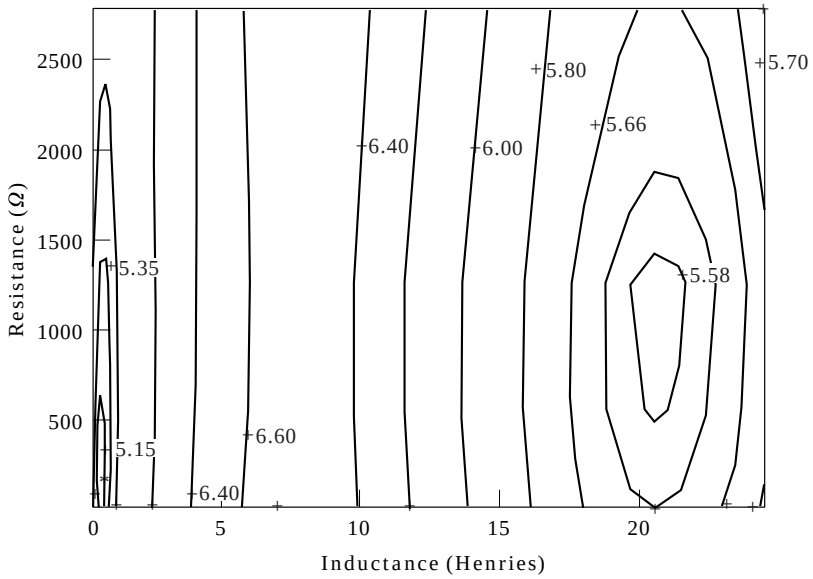

Figure 15. Contour of the cost function J under the excitation bandwidth 640 Hz: *, optimal resistance and inductance; $J = 5{\cdot}119$.

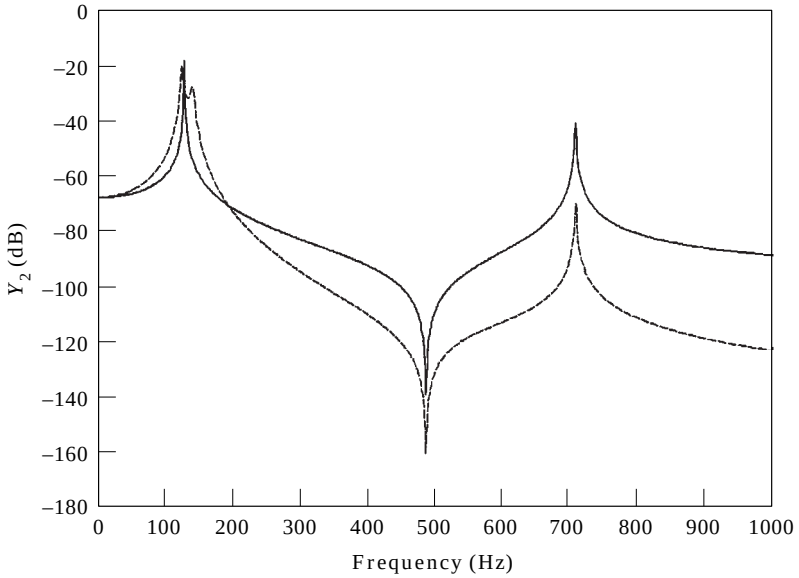

Figure 16. The active authority Y_2 under excitation bandwidth 190 Hz: ——, purely active; – – –, APPN.

APPN system is designed based on the algorithm presented in section 5. The weighting on control efforts S is chosen to be 4×10^{-7}. To evaluate the effects of excitation frequency bandwidth (bandwidth of the Butterworth filter described in section 5.1) on the optimal values of R and L, the contour of the function J for different bandwidths (190, 560 and 640 Hz) are plotted in Figures 13 to 15. Figure 13 shows that there is only one global minimum for J when the excitation frequency bandwidth is 190 Hz. When the bandwidth increases to 560 Hz, the function J will have two local minima with the right one as the global minimum. As the bandwidth increases to 640 Hz, the global minimum will jump from the right to the left region. To explain the phenomenon of this jump, the active authority index Y_2 for bandwidths 190 and 640 Hz are shown in Figures 16 and 17. When the excitation bandwidth is narrow (190 Hz), the optimal R and L are tuned to enhance the active authority around the first mode. Although the Y_2 value of the hybrid system is about 20 dB lower than that of the purely active system for responses above 195 Hz, the system performance will not be affected. This is because the response of the system at higher frequencies is very small when the excitation bandwidth is low and narrow (190 Hz). However, when the excitation frequency increases to 640 Hz, the large response at higher frequencies will affect the objective function very significantly and the optimal R and L will jump to the second mode region.

Figure 18 shows the minimum value of J versus excitation bandwidth for the purely active and APPN cases. A different set of optimal APPN parameters is designed for each given bandwidth. It is clear that the hybrid system outperforms the purely active structure significantly when the bandwidth is low and narrow. However, as the bandwidth increases, the APPN starts to approach the purely active case. This shows that since a shunt is used to enhance the active action

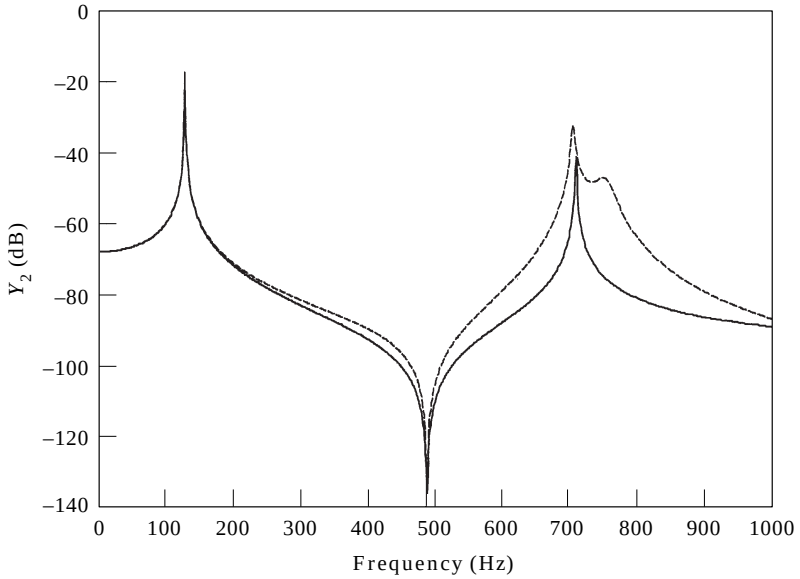

Figure 17. The active authority Y_2 under excitation bandwidth 640 Hz: ——, purely active; – – –, APPN.

around a certain frequency, the results will become less effective when the number of contributing modes greatly exceeds the number of actuators. Nevertheless, the APPN will always outperform the purely active system, as illustrated in Figure 18.

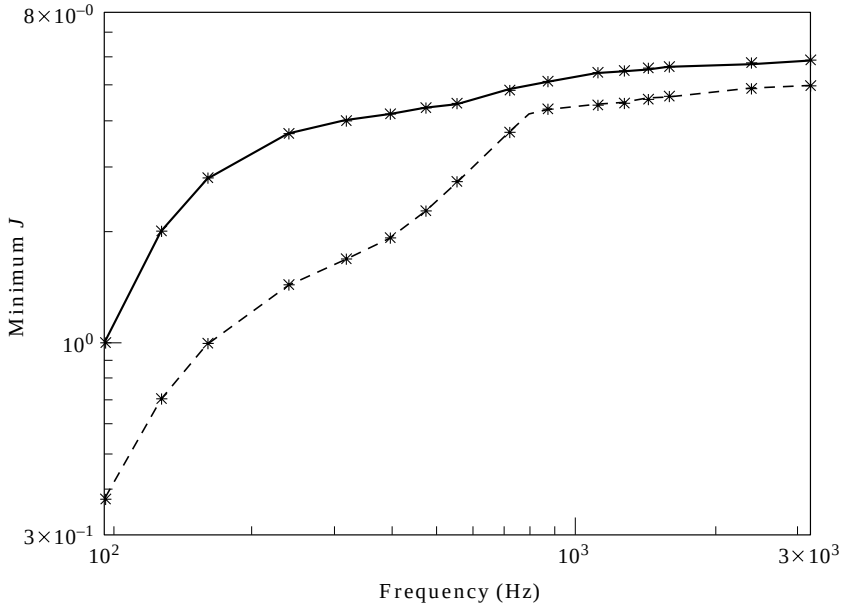

Figure 18. Global minimum value of J versus excitation frequency bandwidth: ——, purely active; – – –, APPN.

7. CONCLUSIONS

This paper presents analysis results that provide understandings of the APPN system. It is shown that the shunt circuit not only can provide passive damping, they can also enhance the active action authority around the tuned frequency. Therefore, the integrated APPN design is more effective than a system with separated active and passive elements. Some of the phenomena predicted in this open-loop analysis have also been observed experimentally [1, 10]. It is also clear that the active authority will be degraded if the inductance is mistuned or if the resistance is too high. Thus, a systematic design/control method is developed to ensure that the passive and active actions are optimally synthesized. This paper also addresses the effects of weighting and frequency bandwidth on the APPN configuration. It is shown that the optimal resistance and inductance values for the hybrid system could be quite different from that of the passive system, especially when the demand on performance is high. It is concluded that the difference between the APPN and purely active cases becomes smaller as the excitation frequency bandwidth increases. One possible method to enhance the system's broadband performance is to increase the number of actuators. Another approach is to integrate the APPN design with other broadband damping elements, such as active constrained layer damping layers [11].

ACKNOWLEDGMENT

This research is supported by the Office of Naval Research.

REFERENCES

1. G. Agnes 1994 *Proceedings of SPIE Smart Structures and Materials Conference* **2193**, 24–34. Active/passive piezoelectric vibration suppression.
2. S. P. Kahn and K. W. Wang 1994 *Proceedings of ASME IMECE* **DE-75**, 187–194. Structural vibration controls via piezoelectric materials with active–passive hybrid networks.
3. K. W. Wang and S. Kahn 1998 *Structronic Systems: Smart Structures*, *Devices and Systems*, Part I, Chap. 8, pp. 247–270. World Scientific Publishing Company. Active–passive hybrid structural vibration controls via piezoelectric networks.
4. M. S. Tsai and K. W. Wang 1996 *IOP Journal of Smart Materials and Structure* **5**, 695–703. Control of a ring structure with multiple active–passive hybrid piezoelectrical networks.
5. *IEEE Standard on Piezoelectricity* 1987, ANSI-IEEE Std 176–1987.
6. D. J. Inman 1989 *Vibrations with Control*, *Measurement*, *and Stability*. Englewood-Cliffs, NJ: Prentice-Hall.
7. N. W. Hagood and A. von Flotow 1991 *Journal of Sound and Vibration* **146**, 243–268. Damping of structural vibrations with piezoelectric materials and passive electrical networks.
8. H. Kwakernaak and R. Sivan 1972 *Linear Optimal Control Systems*. New York: Wiley.
9. J. S. Arora 1989 *Introduction to Optimum Design*. New York: McGraw-Hill.

10. M. S. Tsai 1998 *PhD. Thesis*, *The Pennsylvania State University*. Active–passive hybrid piezoelectric network based smart structures for vibration controls.
11. M. S. Tsai and K. W. Wang 1997 *Proceedings of ASME IMECE* **DE-95**/AMD-Vol. 223, 13–24. Integrating active–passive hybrid piezoelectric networks with active constrained layer treatments for structural damping.

APPENDIX A: OPTIMAL PASSIVE R AND L

For easy comparison with the active–passive hybrid system, instead of using the classical procedure [7] to find the optimal passive resistance and inductance, a different method is used. However, the concept and results are quite similar to those proposed in reference [7].

The system equations can be expressed by the state space form

$$\dot{\underline{\mathbf{y}}} = A(R, L)\underline{\mathbf{y}} + B_1\underline{\mathbf{f}}. \tag{A1}$$

Here, the control action $\underline{u}$ is not included since this system is a passive system. The disturbance $\underline{\mathbf{f}}$ can be modelled as the result of passing a Gaussian, white noise process through a second order low pass Butterworth filter. The bandwidth of the filter is defined to be the radian cut-off frequency at which the filter output has a 3-dB attenuation of its value at zero frequency. The equations that describe such a process are

$$\dot{\underline{\mathbf{s}}} = A_f\underline{s} + B_f\underline{d}, \qquad \underline{\mathbf{f}} = C_f\underline{s}, \tag{A2}$$

The inputs in $\underline{d}$ are Gaussian and white. Here, the mean and spectral density of $\underline{d}$ is given by $E[\underline{d}(t)] = 0$ and $E[\underline{d}(t)\underline{d}^T(\tau)] = D(t)\delta(t-\tau)$; $E[\,]$ is the expectation operator.

By defining an augmented state vector as $\underline{\mathbf{x}} = [\underline{\mathbf{y}}\ \underline{\mathbf{s}}]^T$, the overall system state equations become

$$\dot{\underline{\mathbf{x}}} = \begin{bmatrix} A & B_1C_f \\ 0 & A_f \end{bmatrix}\underline{\mathbf{x}} + \begin{bmatrix} 0 \\ B_f \end{bmatrix}\underline{d} = A_a\underline{\mathbf{x}} + B_{1a}\underline{d}. \tag{A3}$$

The cost function is defined as

$$J_t = \lim_{t\to\infty} E[\underline{\mathbf{x}}^T Q_e \underline{\mathbf{x}}]. \tag{A4}$$

Q_e is a positive-semi-definite weighting matrix chosen to be

$$Q_e = \begin{bmatrix} K_b & & & & \\ & 0 & & 0 & \\ & & 0 & & \\ & & & M_b & \\ & 0 & & 0 & \\ & & & & 0 \end{bmatrix}, \tag{A5}$$

Here, $\underline{\mathbf{x}}^T Q_e \underline{\mathbf{x}}$ represents the overall structure energy. With a given set of passive parameters (R and L), the cost function is

$$tr(B_{1a} D B_{1a}^T P_l). \tag{A6}$$

The system response will consist of a state vector with zero mean and a variance given by the solution (P_l) to the Lyapunov equation

$$A_a^T P_l + P_l A_a + Q_e = 0. \tag{A7}$$

Utilizing a sequential quadratic programming algorithm [9], one can determine the optimal passive R and L to minimize J.

APPENDIX B: NOMENCLATURE

A	open-loop system matrix
A_a	augmented system matrix
A_b	cross-sectional area of beam
A_c	cross-sectional area of PZT
A_{cl}	closed-loop system matrix
A_f	Butterworth filter system matrix
B_1	excitation matrix of open-loop system
B_{1a}	excitation matrix of the augmented system
B_2	control matrix of open-loop system
B_{2a}	control matrix of the augmented system
B_f	Butterworth filter input matrix
b_s	width of beam and PZT
C_1	output matrix of system A
C_f	Butterworth filter output matrix
C_{11}^D	elastic modulus of PZT with open circuit
c_b	uniform damping constant
D_a	electrical displacement of the *upper* PZT
D_s	electrical displacement of the *lower* PZT
$\underline{d}$	white noise
E_b	elastic modulus of beam
E_v	electrical field
$E[\,]$	expected value operator
$f(x, t)$	external loading function of the beam
$\underline{\mathbf{f}}$	disturbance input vector
h_b	distance from neutral axis of beam to outside surface of PZT
h_s	distance from neutral axis of beam to outside surface of PZT
h_{31}	piezoelectric constant of PZT
I_b, I_c	moment of inertia of beam and PZT
J	objective function for overall system optimization
J_e	cost function for the stochastic regulator problem
J_c	$b_s(h_s^2 - h_b^2)/2$
K_c	control gains
L	inductance of the PZTs
L_b	length of the beam
P_l	solution of the Lyapunov equation
P_r	solution of the Riccati equation
Q_a	electrical charge of the *upper* PZT
Q_s	electrical charge of the *lower* PZT
Q_e	weighting matrix on states

$\underline{\mathbf{q}}$ generalized displacement vector
R resistance of the PZT
S weighting matrix on control input
t time
$\underline{u}$ control input
V_a external voltage of the PZT
V_c applied voltage
W output covariance matrix
w transverse displacement
x_1 left end of the PZT
x_2 right end of the PZT
$\underline{\mathbf{x}}$ state vector of augmented system A_a
$\underline{\mathbf{y}}$ state vector of open loop system A
$\overline{\rho}_b$, ρ_c density of beam and PZT
β_{33} dielectric constant of PZT
τ mechanical stress
ε mechanical strain